Reports

A Two-Dimensional Analog VLSI Circuit for Detecting Discontinuities in Early Vision

JOHN G. HARRIS, CHRISTOF KOCH,* JIN LUO

A large number of computer vision algorithms for finding intensity edges, computing motion, depth, and color, and recovering the three-dimensional shape of objects have been developed within the framework of minimizing an associated "energy" or "cost" functional. Particularly successful has been the introduction of binary variables coding for discontinuities in intensity, optical flow field, depth, and other variables, allowing image segmentation to occur in these modalities. The associated nonconvex variational functionals can be mapped onto analog, resistive networks, such that the stationary voltage distribution in the network corresponds to a minimum of the functional. The performance of an experimental analog very-large-scale integration (VLSI) circuit implementing the nonlinear resistive network for the problem of two-dimensional surface interpolation in the presence of discontinuities is demonstrated; this circuit is implemented in complementary metal oxide semiconductor technology.

A LARGE CLASS OF VISION ALGORITHMS is based on minimizing an associated "cost functional." Such a variational formalism is attractive because it allows a priori constraints to be explicitly stated. The single most important constraint is that the physical processes underlying image formation, such as depth, orientation, and surface reflectance, change slowly in space. For instance, the depths of neighboring points on a surface are usually similar. Standard regularization algorithms embody this smoothness constraint and lead to quadratic variational functionals with a unique, global maximum (*1, 2*). These quadratic functionals can be mapped onto linear resistive networks, such that the stationary voltage distribution, corresponding to the state of least power dissipation, is equivalent to the solution of the variational functional (*3*). The data consist of currents injected into the appropriate nodes.

Smoothness breaks down, however, at discontinuities caused by occlusions or by differences in the physical processes underlying image formation (such as different surface reflectance properties). Detecting these discontinuities becomes crucial, not only because otherwise smoothness is incorrectly applied but also because the locations of discontinuities are often required for further image analysis and understanding (for example, one can often reliably find the outline of a moving object by detecting discontinuities in the optical flow field). Geman and Geman (*4*) first introduced a class of stochastic algorithms, based on Markov random fields, that explicitly encodes the absence or presence of discontinuities by means of binary variables. Their approach was extended and modified to account for discontinuities in depth, texture, optical flow, and color (*5*). Using Bayes's theorem, we can compute the maximum a posteriori probability distribution by minimizing a nonconvex functional. Constraints, such that discontinuities occur along continuous contours and rarely intersect, can be incorporated into this formalism. The functional is minimized by stochastic optimization techniques, such as simulated annealing. Various deterministic approximations, based on continuation methods or a mean field theory approach, yield next-to-optimal solutions (*6, 7*).

In this report, we discuss a nonlinear resistive network implementing surface smoothing as well as segmentation, an important problem in computer vision (*2*). In the one-dimensional (1-D) case (the 2-D generalization is straightforward), the sparse and noisy depth data d_i are given on a discrete grid. Associated with each lattice point is the value of the recovered surface f_i and a binary line discontinuity ℓ_i. When the surface is expected to be smooth (with a first-order, membrane-type stabilizer) except at isolated discontinuities, the functional to be minimized is given by:

$$J(f,\ell) = \lambda\sum_i (f_{i+1} - f_i)^2(1 - \ell_i) + \frac{1}{2\sigma^2}\sum_i (d_i - f_i)^2 + \alpha\sum_i \ell_i \qquad (1)$$

where σ^2 is the variance of the additive Gaussian noise process assumed to corrupt the data d_i, and λ and α are free parameters (*8*). The first term on the right implements the piecewise smooth constraint: if all variables, with the exception of f_i, f_{i+1}, and ℓ_i, are held fixed and $\lambda(f_{i+1} - f_i)^2 < \alpha$, then it is "cheaper" to pay the price $\lambda(f_{i+1} - f_i)^2$ and to set $\ell_i = 0$ than to pay the larger price α; if the gradient becomes too steep, $\ell_i = 1$, and the surface is segmented at that location.

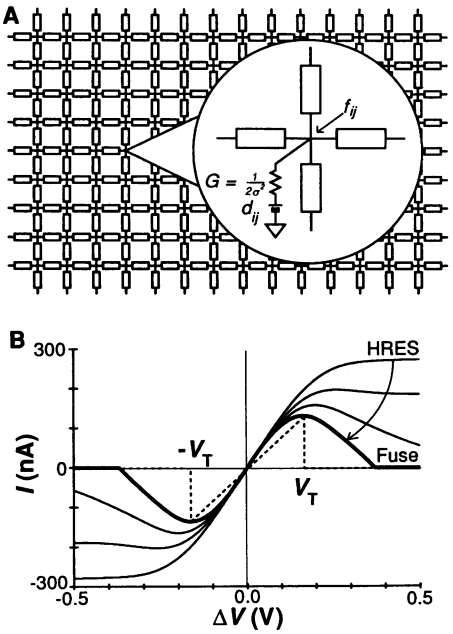

Fig. 1. (**A**) Schematic diagram for our 20 by 20 pixel surface interpolation and smoothing chip. A rectangular mesh of resistive fuse elements (shown as rectangles) provides the smoothing and segmentation ability of the network. The data are given as battery values d_{ij} with the conductance G connecting the battery to the grid set to $G = 1/2\sigma^2$, where σ^2 is the variance of the additive Gaussian noise assumed to corrupt the data. If no data are available, $G = 0$. The output is the voltage f_{ij} at each node. Parasitic capacitances (not shown) provide the dynamics. We usually assume a zero slope boundary condition along the boundary. Data are read in or out by means of additional scanning circuitry (not shown). This circuit converges to a minimum of the functional J of Eq. 1. (**B**) Measured I-V relation for different settings of the resistive fuse. We can continuously vary the I-V curve from the hyperbolic tangent of Mead's saturating resistor (HRES) to that of an analog fuse. The I-V curve of a binary fuse is also illustrated (dashed line). For a voltage of less than $V_T = \sqrt{\alpha/\lambda}$ across this two-terminal device, the circuit acts as a resistor with conductance λ. Above V_T, the current is either abruptly set to zero (binary fuse) or smoothly goes to zero (analog fuse). Independent voltage control lines allow us to change both λ (over four orders of magnitude) and V_T (from 50 to 500 mV).

Computation and Neural Systems Program, California Institute of Technology, Pasadena, CA 91125.

*To whom correspondence should be addressed at the Division of Biology 216-76, California Institute of Technology, Pasadena, CA 91125.

The second term, with the sum including only those locations i where data exist, forces the surface f to be close to the measured data d. How close depends on the estimated magnitude of the noise, in this case, on σ^2. The final surface f is the one that best satisfies the conflicting demands of piecewise smoothness and fidelity to the measured data.

Instead of resorting to stochastic search techniques to find the global minimum of the 2-D generalization of Eq. 1, we use a deterministic approximation and map the functional J onto the circuit shown in Fig. 1A. The stationary voltage at every grid point then corresponds to f_{ij}. If data exist at location i, j, a battery is set to d_{ij}, and the conductance between the battery and the grid is set to $G = 1/(2\sigma^2)$. If no data exist, $G = 0$. In the absence of any discontinuities (all $\ell = 0$), smoothness is implemented via a conductance of value λ connecting neighboring grid points; that is, the elongated rectangles in Fig. 1 can simply be considered resistors. The cost functional J can then be interpreted as the power dissipated by the circuit. If parasitic capacitors are added to the circuit, J acts as a Lyapunov function of the system and the stationary voltage distribution corresponds to the smooth surface (*9*).

We designed a two-terminal nonlinear device, which we call a "resistive fuse," to implement piecewise smoothness (Fig. 1B). If the magnitude of the voltage drop across the device is less than $V_T = (\alpha/\lambda)^{1/2}$, the current through the device is proportional to the voltage, with a conductance of λ. This implements smoothness. If V_T is exceeded, the fuse breaks and the current goes to zero. The operation of the fuse is fully reversible. We use an "analog fuse" with the current-voltage (I-V) curve shown in Fig. 1B, implementing a continuous version of the binary line discontinuities. Its exact form can be derived from mean field theory (*6, 10, 11*). If the internal dynamics of the resistive fuse can be neglected, then it can be proven that the network will not oscillate but rather will settle into a local minimum. The associated Lyapunov function is the electrical co-content (*12*).

We built a 20 by 20 pixel very-large-scale integration (VLSI) chip, using the subcircuit types and design practices developed by Mead (*13*). The slope λ and the voltage threshold $(\alpha/\lambda)^{1/2}$ of all fuses can be set by off-chip voltage inputs. Furthermore, the I-V curve of a fuse can be continuously varied from that of a saturating resistor to that of an "analog fuse" (Fig. 1B), effectively implementing a continuation method for minimizing the nonconvex functional (*14*). Figure 2 shows experimental data from our chip. The input data correspond to a central tower on a flat plane corrupted by Gaussian noise (Fig. 2, A and D). Figure 2, B and E, illustrates the resultant voltage distribution if the "fuses" are set to act as saturating resistors. The tower merges into the plane, because there are no discontinuities to prevent smoothing from occurring. Figure 2, C and F, shows that changing the I-V curve from that of a saturating resistor to that of an analog fuse (Fig. 1B) enables the network to clearly segment the tower from the background. Numerical analysis as well as our empirical studies have shown that the smoothing abilities of resistive networks are robust to variations (caused by process variations) in the value of the resistances across the chip (*15*). Furthermore, point defects, such as the one shown in Fig. 2C, induce line processes to break, thereby preventing the error from propagating.

Computer simulations have shown that a resistive network with such fuses can recover the optical flow in the presence of motion discontinuities (*16*). We are currently building a variety of such resistive networks for finding edges and computing depth and optical flow in the presence of discontinuities. These circuits are robust and accurate enough to allow for simple navigation tasks such as following edges or tracking moving light sources when mounted onto toy cars operating in a laboratory environment (*17*). We have now successfully demonstrated all the circuit elements necessary to perform on-chip image acquisition and processing—photoreceptors, resistive grids, and resistive fuses. It appears that real-time, small, power-lean (*18*) and robust analog computers are making a limited comeback in the form of highly dedicated, smart vision chips (*19*).

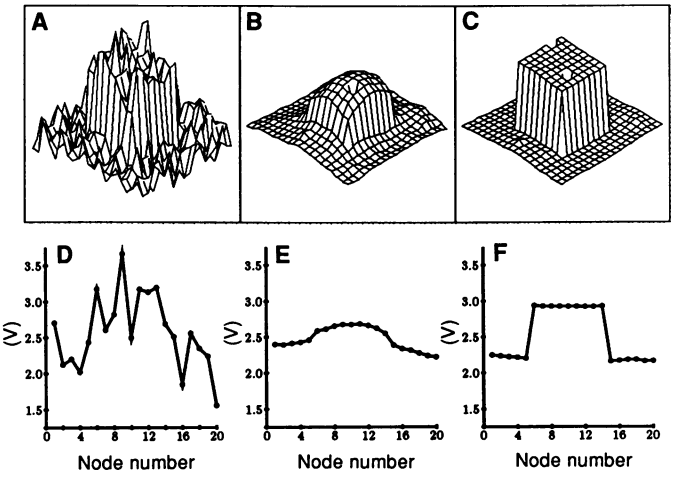

Fig. 2. Experimental data from our chip. We use as input data a tower (corresponding to d_{ij} = 3.0 V) rising from a plane (corresponding to 2.0 V) with superimposed Gaussian noise. (**A**) The input with the variance of the noise set to 0.2 V. (**B**) The voltage output with the fuse configured as a saturating resistance. (**C**) The voltage output when the I-V curve of the fuse has been changed from the saturating resistance to that of the analog fuse (following the arrow in Fig. 1B) while at the same time the conductance λ has been increased. (**D–F**) The same behavior along a horizontal slice across the chip for $\sigma^2 = 0.4$ V. The smoothing and segmentation abilities of the fuses are obvious. The amplitude of the noise in the last case (40% of the amplitude of the voltage step) is so large that a single filtering step on the input (D) will fail to detect the tower. Cooperativity and hysteresis are required for optimal performance. Notice the "bad" pixel in the middle of the tower [in (C)]. Its effect is localized, however, to a single element.

REFERENCES AND NOTES

1. B. K. P. Horn and B. G. Schunck, *Artif. Intell.* **17**, 185 (1981); E. C. Hildreth, *The Measurement of Visual Motion* (MIT Press, Cambridge, MA, 1984); T. Poggio, V. Torre, C. Koch, *Nature* **317**, 314 (1985); T. Poggio, H. Voorhees, A. Yuille, *Artif. Intell. Lab. Memo No. 833* (Massachusetts Institute of Technology, Cambridge, 1986).
2. W. E. L. Grimson, *From Images to Surfaces* (MIT Press, Cambridge, MA, 1981).
3. B. K. P. Horn, *Comput. Graph. Image Process.* **3**, 111 (1974); T. Poggio and C. Koch, *Proc. R. Soc. London Ser. B* **226**, 303 (1985).
4. S. Geman and D. Geman, *IEEE Trans. Pattern Anal. Mach. Intell.* **6**, 721 (1984).
5. J. Marroquin, S. Mitter, T. Poggio, *J. Am. Stat. Assoc.* **82**, 76 (1987); T. Poggio, E. B. Gamble, J. J. Little, *Science* **242**, 436 (1988); J. Hutchinson, C. Koch, J. Luo, C. Mead, *IEEE Trans. Comput.* **21**, 52 (1988); P. B. Chou and C. M. Brown, in *Proceedings of the Image Understanding Workshop* (Morgan Kaufmann, San Mateo, CA, 1988), pp. 214–221.
6. C. Koch, J. Marroquin, A. Yuille, *Proc. Natl. Acad. Sci. U.S.A.* **83**, 4263 (1986); A. Blake and A. Zisserman, *Visual Reconstruction* (MIT Press, Cambridge, MA, 1987); A. Blake, *IEEE Trans. Pattern Anal. Mach. Intell.* **11**, 2 (1989); D. Geiger and F. Girosi, *Artif. Intell. Lab. Memo No. 1114* (1989).
7. D. Terzopoulos, *IEEE Trans. Pattern Anal. Mach. Intell.* **8**, 413 (1986).
8. In regularization theory, λ is usually set to 1. Notice that the shape of J is unique up to a multiplicative constant.
9. We previously demonstrated a 48 by 48 pixel hexagonal analog VLSI circuit implementing surface interpolation and smoothing: J. Luo, C. Koch, C. Mead, in *Neural Networks*, B. D. Shriver, Ed. (Computer Science Press, Washington, DC, in press); J. G. Harris [in *Neural Information Processing Systems 1*, D. Touretzky, Ed. (Morgan Kaufmann, Palo Alto, CA, 1989), pp. 687–694] has built a 1-D second-order surface interpolation chip.
10. A. Lumsdaine, J. Wyatt, I. Elfadel, in *Proceedings of the IEEE International Symposium on Circuits and Systems* (New Orleans, LA, 1990) (IEEE, New York, 1990), pp. 987–991.
11. In the mean field approximation, the current through an "analog fuse" is given by $I = f(V) = \lambda V[1 + e^{\beta(\lambda V^2 - \alpha)}]$, where V is the voltage

across the fuse and β is a free parameter corresponding to the temperature. P. Perona and J. Malik [in *Proceedings of the IEEE International Symposium on Circuits and Systems* (Espoo, Finland, 1988) (IEEE, New York, 1988), pp. 2565–2568] have simulated similar elements using anisotropic diffusion.
12. For a two-terminal, voltage-controlled resistor characterized by $I = f(V)$, the co-content is defined as $J(V) = \int_0^V f(V')dV'$. For a linear resistor $I = GV$ and $J = GV^2/2$, half of the dissipated power $P = GV^2$. For stability results, see J. G. Harris, C. Koch, J. Luo, and J. Wyatt [in *Analog VLSI Implementations of Neural Systems*, C. Mead and M. Ismail, Eds. (Kluwer, Norwell, MA, 1989), pp. 27–56].
13. See C. Mead, *Analog VLSI and Neural Systems* (Addison-Wesley, Reading, MA, 1989). Our chip contains about 40,000 transistors, uses a 2.0-μm *n*-well complementary metal oxide semiconductor process, and was fabricated via MOSIS, the government-sponsored silicon foundry. Gate voltages are typically around 1.0 V.
14. J. M. Ortega and W. C. Rheinboldt, *Iterative Solution of Nonlinear Equations in Several Variables* (Academic Press, New York, 1970).
15. J. M. Hutchinson and C. Koch, in *Neural Networks for Computing*, J. Denker, Ed. (American Institute of Physics, New York, 1986), pp. 235–240; W. C. Elmore, *J. Appl. Phys.* **19**, 55 (1948).
16. J. G. Harris, C. Koch, E. Staats, J. Luo, *Int. J. Comput. Vision*, in press.
17. C. Koch, J. Harris, J. Luo, A. Hsu, T. Horiuchi, in *Neural Information Processing Systems 2*, D. Touretzky, Ed. (Morgan Kaufmann, Palo Alto, CA, in press).
18. Our analog circuitry consumes < 0.1 mW of power.
19. For a review of analog circuits for vision, see C. Koch, *Neural Comput.* **1**, 184 (1989); B. K. P. Horn, *Artif. Intell. Lab. Memo No. 1071* (1989).
20. We thank C. Mead for support. All chips were fabricated through MOSIS with the support of the Defense Advanced Research Projects Agency. Our research is supported by NSF grant IST-8700064, an NSF Presidential Young Investigator Award (to C.K.), a grant from the Office of Naval Research, DDF-II funds from the Jet Propulsion Laboratory at the California Institute of Technology, and funds from the Rockwell International Science Center and the Hughes Aircraft Artificial Intelligence Center. J.G.H. is a Hughes Aircraft Corporation fellow.

28 December 1989; accepted 12 April 1990

Structural and Electronic Role of Lead in $(PbBi)_2Sr_2CaCu_2O_8$ Superconductors by STM

XIAN LIANG WU, ZHE ZHANG, YUE LI WANG, CHARLES M. LIEBER*

The structural and electronic effects of lead substitution in the high-temperature superconducting materials $Pb_xBi_{2-x}Sr_2CaCu_2O_8$ have been characterized by scanning tunneling microscopy (STM) and scanning tunneling spectroscopy (STS). Large-area STM images of the Bi(Pb)–O layers show that lead substitution distorts and disorders the one-dimensional superlattice found in these materials. Atomic-resolution images indicate that extra oxygen atoms are present in the Bi(Pb)–O layers. STS data show that the electronic structure of the Bi(Pb)–O layers is insensitive to lead substitution within ±0.5 electron volt of the Fermi level; however, a systematic decrease in the density of states is observed at ≈1 electron volt above the Fermi level. Because the superconducting transition temperatures are independent of x(Pb) ($x \leq 0.7$), these microscopic STM and STS data suggest that the lead-induced electronic and structural changes in the Bi(Pb)–O layer do not perturb the electronic states critical to forming the superconducting state in this system.

SUBSTITUTION OF METALS IN THE RECENTLY discovered high-temperature superconductors has been used extensively both to probe factors that determine superconductivity and to prepare new materials (*1*). A case in point is Pb substitution in the Bi–O layers of Bi-Sr-Ca-Cu oxide materials (Fig. 1). Since Sunshine and co-workers first reported that the substitution of Pb enhances the superconducting onset temperature from 85 to 107 K in multiphase ceramic samples (*2*), numerous investigations of this chemical modification have been reported (*3–13*). In polycrystalline $(PbBi)_2Sr_2Ca_{n-1}Cu_nO_{2n+4}$ materials, Pb substitution has been found to favor the formation of the 110 K, $n = 3$ (2223) phase versus the 85 K, $n = 2$ (2212) phase (*8, 9*). In addition, diffraction studies have shown that the prominent one-dimensional incommensurate superstructure observed in $Bi_2Sr_2CaCu_2O_8$ changes upon substitution of Pb, although the details of these changes appear to be sample-dependent (*3–7*). Hence, it is not yet known how Pb substitution affects the intrinsic superconducting properties of these materials.

To probe directly the structural and electronic effects of Pb substitution, we studied high-quality, single-crystal $Pb_xBi_{2-x}Sr_2CaCu_2O_8$ ($x = 0$, 0.3, or 0.7) materials by scanning tunneling microscopy (STM) and scanning tunneling spectroscopy (STS). STM and STS are ideal techniques for characterizing the structural and electronic effects of Pb substitution because Pb primarily replaces Bi in the Bi–O layers (*10, 11*) and

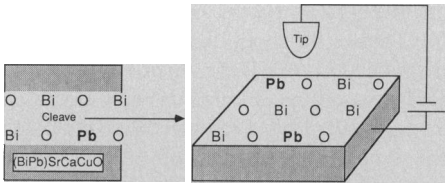

Fig. 1. Schematic view of $Pb_xBi_{2-x}Sr_2CaCu_2O_8$ showing the Bi(Pb)–O double layer and the surface STM geometry in these experiments. The bulk structure consists of a repeating sequence of Bi(Pb)–O, Sr–O, Cu–O, Ca, Cu–O, Sr–O, and Bi(Pb)–O layers as described by Sunshine *et al.* (*2*).

the $Pb_xBi_{2-x}Sr_2CaCu_2O_8$ crystals can be cleaved to expose a Bi(Pb)–O layer at the surface (Fig. 1).

Single-crystal samples with the nominal composition $Pb_xBi_{2-x}Sr_2CaCu_2O_8$ ($x = 0$, 0.3, or 0.7) were grown from melts rich in CuO. Briefly, a homogeneous mixture of PbO, Bi_2O_3, $SrCO_3$, $CaCO_3$, and CuO powders was heated at 980°C for 10 hours, cooled at 2°C per hour to 800°C, and then furnace-cooled to room temperature. Bulk and surface analyses demonstrated that Pb was incorporated into these crystals at close to the Pb/Bi stoichiometry of the melts, although the Sr and Ca concentrations were slightly deficient with respect to the ideal 2212 formula. Single-crystal x-ray diffraction studies further showed that the crystal structures of the x(Pb) = 0 to 0.7 materials are the same (*14*); these data are in agreement with the results of earlier reports (*4, 8, 9*). The values of the superconducting transition temperature T_c (zero resistance) determined from dc resistivity measurements on at least five crystals are (T_c ± 1 SD) 85 ± 4, 88 ± 3, and 85 ± 2 K for the x = 0, 0.3, and 0.7 compositions, respectively. The sharp transitions observed for our materials [ΔT(90 to 10%) = 3 to 4 K] are indicative of high-quality materials. Furthermore, magnetic measurements (Meissner effect) demonstrate that the x(Pb) = 0, 0.3, and 0.7 crystals have similar bulk superconducting fractions. These structural, electrical, and magnetic data indicate that our crystals have reproducible macroscopic properties and hence are ideal for high-resolution STM studies.

All of the STM and STS studies of the $Pb_xBi_{2-x}Sr_2CaCu_2O_8$ materials were performed in an Ar-filled glove box equipped with a purification system that reduced the concentrations of H_2O and O_2 to below 1 ppm. The glove box environment, $PO_2 \approx 10^{-3}$ torr, was used to reduce the possibility of O_2 loss from the surface of the materials that may occur in ultrahigh vacuum (*12, 15*), at $PO_2 = 10^{-10}$ to 10^{-11} torr. The modified tunneling microscopes used in

Department of Chemistry, Columbia University, New York, NY 10027.

*To whom correspondence should be addressed.